Cellular/Molecular

Disruption of *tmc1/2a/2b* Genes in Zebrafish Reveals Subunit Requirements in Subtypes of Inner Ear Hair Cells

Eliot T. Smith,[1] Itallia Pacentine,[2] Anna Shipman,[1] Matthew Hill,[2] and Teresa Nicolson[1]

[1]Department of Otolaryngology Head and Neck Surgery, Stanford School of Medicine, Stanford University, Stanford, California 94305, and [2]Oregon Hearing Research Center, Oregon Health and Science University, Portland, Oregon 97239

Detection of sound and head movement requires mechanoelectrical transduction (MET) channels at tips of hair-cell stereocilia. In vertebrates, the transmembrane channel-like (TMC) proteins TMC1 and TMC2 fulfill critical roles in MET, and substantial evidence implicates these TMCs as subunits of the MET channel. To identify developmental and functional roles of this Tmc subfamily in the zebrafish inner ear, we tested the effects of truncating mutations in *tmc1*, *tmc2a*, and *tmc2b* on *in vivo* mechanosensation at the onset of hearing and balance, before gender differentiation. We find that *tmc1/2a/2b* triple-mutant larvae cannot detect sound or orient with respect to gravity. They lack acoustic-evoked behavioral responses, vestibular-induced eye movements, and hair-cell activity as assessed with FM dye labeling and microphonic potentials. Despite complete loss of hair-cell function, *tmc* triple-mutant larvae retain normal gross morphology of hair bundles and proper trafficking of known MET components Protocadherin 15a (Pcdh15a), Lipoma HMGIC fusion partner-like 5 (Lhfpl5), and Transmembrane inner ear protein (Tmie). Transgenic, hair cell-specific expression of Tmc2b-mEGFP rescues the behavioral and physiological deficits in *tmc* triple mutants. Results from *tmc* single and double mutants evince a principle role for Tmc2a and Tmc2b in hearing and balance, respectively, whereas Tmc1 has lower overall impact. Our experiments reveal that, in developing cristae, hair cells stratify into an upper, Tmc2a-dependent layer of teardrop-shaped cells and a lower, Tmc1/2b-dependent tier of gourd-shaped cells. Collectively, our genetic evidence indicates that auditory/vestibular end organs and subsets of hair cells therein rely on distinct combinations of Tmc1/2a/2b.

Key words: **auditory/vestibular system; hair cells; inner ear; mechanoelectrical transduction; mechanosensation; TMC proteins**

Significance Statement

We assessed the effects of *tmc1/2a/2b* truncation mutations on mechanoelectrical transduction (MET) in the inner-ear hair cells of larval zebrafish. *tmc* triple mutants lacked behavioral responses to sound and head movements, while further assays demonstrated no observable mechanosensitivity in the *tmc1/2a/2b* triple mutant inner ear. Examination of *tmc* double mutants revealed major contributions from Tmc2a and Tmc2b to macular function; however, Tmc1 had less overall impact. FM labeling of lateral cristae in *tmc* double mutants revealed the presence of two distinct cell types, an upper layer of teardrop-shaped cells that rely on Tmc2a, and a lower layer of gourd-shaped cells that rely on Tmc1/2b.

Introduction

Central to senses of hearing and balance, hair cells rely on the mechanoelectrical transduction (MET) protein complex to convert mechanical stimuli into an electrical signal. The MET complex, resident at the tips of hair-cell stereocilia, consists of a cation-permeable channel and associated binding partners (Corey and Hudspeth, 1979; Hudspeth, 1982; Beurg et al., 2009; for review, see Ó Maoiléidigh and Ricci, 2019). An extracellular filament, the tip-link, tethers each MET channel to an adjacent, taller stereocilium, forming the MET apparatus (Pickles et al., 1984; Assad et al., 1991). Upon mechanical deflection of stereocilia, increased tension on tip-links opens MET channels causing depolarization. This mechanism relies on concerted function of several protein subunits.

The mammalian MET complex comprises at least five distinct proteins: Protocadherin15 (PCDH15) (Kazmierczak et al., 2007), Lipoma HMGIC fusion partner-like 5 (LHFPL5) (Xiong et al., 2012; Mahendrasingam et al., 2017), Transmembrane inner ear protein (TMIE) (Zhao et al., 2014; Pacentine and Nicolson, 2019), and Transmembrane Channel-like (TMC) proteins

Received Jan. 15, 2020; revised Apr. 14, 2020; accepted Apr. 16, 2020.

Author contributions: E.T.S., I.P., and T.N. designed research; E.T.S., I.P., A.S., and M.H. performed research; E.T.S., I.P., A.S., M.H., and T.N. analyzed data; E.T.S. wrote the first draft of the paper; E.T.S., I.P., A.S., and T.N. edited the paper; E.T.S. wrote the paper.

This work was supported by National Institute on Deafness and Other Communication Disorders R01 DC013572 and DC013531 to T.N.

The authors declare no competing financial interests.

Correspondence should be addressed to Teresa Nicolson at tnicolso@stanford.edu.

https://doi.org/10.1523/JNEUROSCI.0163-20.2020

TMC1 and TMC2 (referred to as TMC1/2) (Kawashima et al., 2011; Pan et al., 2013; Kurima et al., 2015). PCDH15 forms the lower portion of the tip-link (Kazmierczak et al., 2007; Indzhykulian et al., 2013) and connects with TMC1/2 via protein-protein interactions (Kazmierczak et al., 2007; Indzhykulian et al., 2013; Maeda et al., 2014). LHFPL5 cotransports with PCDH15, where it resides as part of the MET complex (Xiong et al., 2012). TMIE also localizes to the tips of stereocilia (Zhao et al., 2014) and, in zebrafish, is required for proper localization of Tmc1/2b (Pacentine and Nicolson, 2019). Although unclear whether PCDH15, LHFPL5, or TMIE forms part of the pore, accumulating evidence implicates TMC1/2 as principal pore-forming subunits of MET channels (Kawashima et al., 2011, 2015; Nakanishi et al., 2014; Kurima et al., 2015; Chou et al., 2017; Beurg et al., 2018, 2019; Pan et al., 2018; Fettiplace and Nam, 2019; Goldring et al., 2019; Jia et al., 2020). Mutations in *TMC1/2* affect conductance and Ca^{2+} permeability properties of the MET channel, with at least 40 identified *TMC1* alleles causing human deafness (Kawashima et al., 2015). Hair cells express TMC1/2 concurrent with onset of MET (Géléoc and Holt, 2003; Kawashima et al., 2011; Scheffer et al., 2015), and TMC1/2 localize with other MET components at stereocilia tips (Kurima et al., 2015; Mahendrasingam and Furness, 2019). Despite the absence of crystallographic data, modeling indicates structural similarity between TMC1/2 and Transmembrane protein 16a (TMEM16A) ion channels (Pan et al., 2018), and recent evidence demonstrates that TMC1/2 can form mechanosensitive channels in liposomes (Jia et al., 2020).

Previous *in vivo* studies investigating MET complex components in zebrafish elucidated functions of Pcdh15a (Maeda et al., 2014, 2017), Lhfpl5a (Maeda et al., 2017), and Tmie (Gleason et al., 2009; Pacentine and Nicolson, 2019). Zebrafish have two *TMC2* paralogs, *tmc2a/2b*, due to genetic duplication in teleost fish (Maeda et al., 2014). *tmc1/2a/2b* are expressed in the inner ear and lateral-line organ; *tmc2a* is present at earlier stages and higher levels in the ear, whereas *tmc2b* is more predominantly expressed in the lateral line (Maeda et al., 2014). To date, studies of *tmc* disruption in zebrafish have shown that the *tmc2* gene duplicates are required for function in the lateral line and in the macular organs of the inner ear, where mutation of both *tmc2a* and *tmc2b* abolished hair-cell activity (Chou et al., 2017; Chen et al., 2020). Nevertheless, the role of each tmc gene in the inner ear has not been explored comprehensively with respect to hearing and balance, especially regarding functional contributions in specific subtypes of hair cells.

To identify the specific roles of Tmc1/2 in inner-ear hair cells, we generated *tmc1/2a/2b* single-, double-, and triple-mutant zebrafish lines using reverse genetic methods. We examined behavioral, cellular, and physiological consequences of loss of *tmc* function at the onset of hearing and balance, revealing differential effects on hair-cell subpopulations in the larval inner ear.

Materials and Methods

Zebrafish care and use

We maintained zebrafish lines for all mutant alleles and transgenes in Top Long Fin (TLF) and Tübingen WT backgrounds. Breeding stocks were housed at 28°C and animal husbandry followed standard zebrafish methods for laboratory utilization (Westerfield, 2000), as approved and overseen by the Institutional Animal Care and Use Committees at both Oregon Health and Sciences University and Stanford University. The experiments used zebrafish larvae ≤6 days post fertilization (dpf) before gender differentiation occurs. Embryos and larvae grew in E3 medium (0.33 mM $CaCl_2$, 0.17 mM KCl, 0.33 mM $MgSO_4$, and 5 mM NaCl) incubated at 28.5°C. When appropriate, larvae were anesthetized in E3 + 0.03% 3-amino benzoic acid ethylester (MESAB, Western Chemical) to minimize pain and distress.

Generation of Tmc *mutant lines and transgenic lines*

A zebrafish line heterozygous for the $tmc2a^{Ex4,\ -23bp}$ allele (see Fig. 1*A*) was produced by PNA Bio using TALEN-based gene-editing techniques (Bedell et al., 2012; Bedell and Ekker, 2015). Separately, a carrier line for the $tmc2b^{sa8817}$ allele (see Fig. 1*A*) was generated by the Wellcome Trust Sanger Institute Zebrafish Mutation Project (Kettleborough et al., 2013) and obtained from the Zebrafish International Resource Center.

The $tmc2a^{Ex4,\ -23bp}/tmc2b^{sa8817}$ dual-carrier line was produced by crossing $tmc2a^{Ex4,\ -23bp}$ and $tmc2b^{sa8817}$ lines. The *tmc1*, *tmc2a*, and *tmc2b* genes all reside on chromosome 5; however, high frequency of *tmc2a* homologous recombination enabled transfer of $tmc2a^{Ex4,\ -23bp}$ to the chromosome positive for $tmc2b^{sa8817}$ when generating this line.

We generated mutant $tmc1^{Ex3,\ +1bp(1)}$, $tmc1^{Ex3,\ +1bp(2)}$, and $tmc1^{Ex3,\ -5bp}$ alleles (see Fig. 1*A*) using CRISPR-Cas9 with nonhomologous end joining (Hwang et al., 2013a,b). The web-based tool CHOPCHOP (Montague et al., 2014; Labun et al., 2016, 2019) provided a ranking of target site candidates in the *tmc1* gene. We selected the target sequence 5′-TCAGAGAAAAGAACAAACGA-3′ in the third exon (see Fig. 1*A*) based on its high ranking in CHOPCHOP, its early site of truncation (exon 3 of 20), and consideration of putative alternate start site ATG codons. Integrated DNA Technologies synthesized the *tmc1*-specific guide RNA using their Alt-R technology and two-part crRNA:tracrRNA gRNA format.

To form a ribonucleoprotein complex for injection, we combined the gRNA with recombinant Cas9 protein plus nuclear localization signal (Cas9-NLS) (PNA Bio), per the manufacturers' protocols. Equimolar concentrations of the tracrRNA and *tmc1*-specific crRNA (16.6 μM) were combined in nuclease-free Integrated DNA Technologies duplex buffer, heated to 95°C for 5 min, and equilibrated to room temperature to form the *tmc1*-specific gRNA. Separately, lyophilized Cas9-NLS in 20 mM HEPES, 150 mM KCl, 1% sucrose, pH 7.5, was reconstituted to 1 μg/μl (6.14 μM) with nuclease-free H_2O. Finally, equal volumes (1 μl each) of *tmc1* gRNA and Cas9-NLS were mixed (a 2.5:1 molar ratio), heated to 37°C for 10 min, and equilibrated to room temperature. The ribonucleoprotein complex was injected (1-2 nl per embryo) into the yolk of embryos, as specified below, within 1 h after fertilization.

We injected WT TLF embryos to generate the $tmc1^{Ex3,\ -5bp}$ allele for single mutants. Embryos heterozygous for the $tmc2a^{Ex4,\ -23bp}/tmc2b^{sa8817}$ double-mutant chromosome were injected to yield a $tmc1^{Ex3,\ +1bp(1)}/tmc2a^{Ex4,\ -23bp}/tmc2b^{sa8817}$ triple-mutant chromosome and $tmc1^{+Ex3,1\ bp(2)}/\ tmc2a^{Ex4,\ -23bp}$ double-mutant chromosome. High-frequency homologous recombination of *tmc2a* and tight linkage of the *tmc1* and *tmc2b* genes (5 kb apart) allowed us to produce the double-mutant combination $tmc1^{Ex3,\ +1bp(1)}/tmc2b^{sa8817}$ from the $tmc1^{Ex3,\ +1bp(1)}/tmc2a^{Ex4,\ -23bp}/tmc2b^{sa8817}$ line.

The transgenic lines *Tg(myo6b:β-actin-mEGFP-pA)*, *Tg(myo6b:tmie-mEGFP-pA)*, *Tg(myo6b:tmc2b-mEGFP-pA)*, *Tg(myo6b:pcdh15aCD3-mEGFP-pA)*, and *Tg(myo6b:mEGFP-lhfpl5a-pA)*, all previously characterized (Kindt et al., 2012; Erickson et al., 2017; Pacentine and Nicolson, 2019), were each mated to $tmc1^{Ex3,\ +1bp(1)}/tmc2a^{Ex4,\ -23bp}/tmc2b^{sa8817}$ triple heterozygotes to yield *tmc* triple-heterozygous lines for each transgene. The myosin6b promoter (*myo6b*) drives expression of the transgenes only in hair cells.

Attempts to make $tmc1^{Ex3,\ +1bp(1)}/tmc2a^{Ex4,\ -23bp}/tmc2b^{sa8817}$ triple-heterozygous lines for the transgenes *Tg(myo6b:tmc1-mEGFP-pA)* and *Tg(myo6b:tmc2a-mEGFP-pA)* failed due to technical issues. The *Tg(myo6b:tmc1-mEGFP-pA)* transgenic line described by Erickson et al. (2017) was crossed with the $tmc1^{Ex3,\ +1bp(1)}/tmc2a^{Ex4,\ -23bp}/tmc2b^{sa8817}$ triple-mutant line. We later discovered, however, that *Tg(myo6b:tmc1-mEGFP-pA)* was carried by chromosome 5 containing WT *tmc1/2a/2b* alleles, precluding generation of $tmc1^{Ex3,\ +1bp(1)}/tmc2a^{Ex4,\ -23bp}/tmc2b^{sa8817}$ triple-mutant larvae carrying this transgene. The *Tg(myo6b:tmc2a-mEGFP-pA)* construct failed to express Tmc2a-mEGFP.

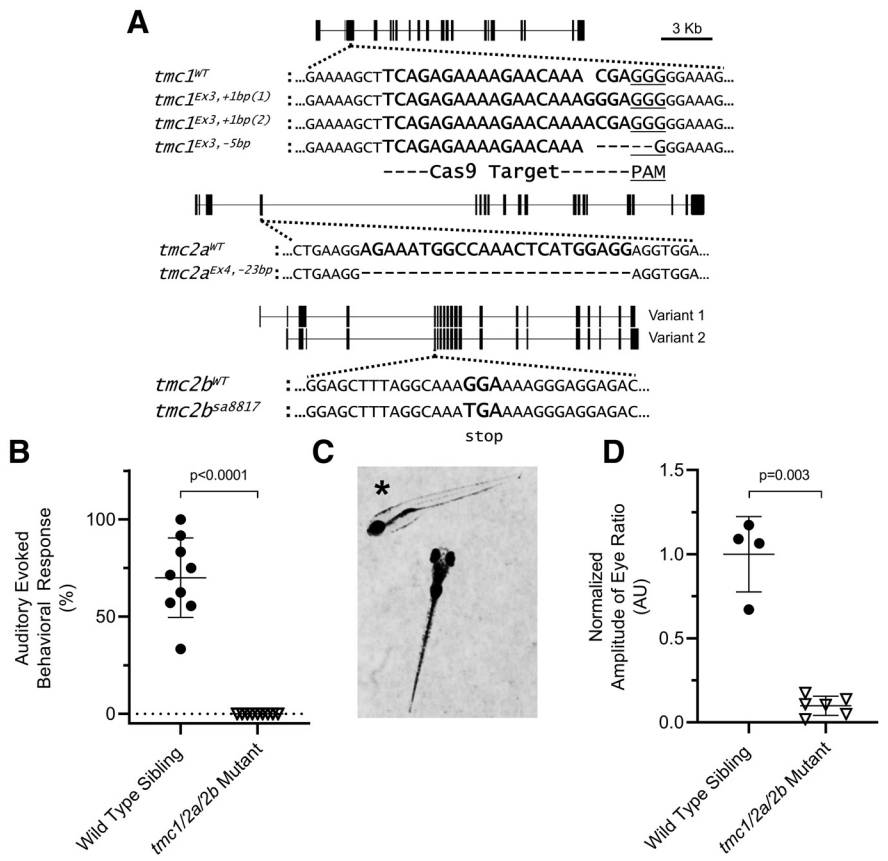

Figure 1. *tmc1/2a/2b* triple-mutant larvae have auditory/vestibular defects. ***A***, Truncation mutant alleles are shown for *tmc1* (frame shift), *tmc2a* (frame shift), and *tmc2b* (point mutation) genes. A diagram of each gene is included. Vertical bars represent exons. Horizontal lines indicate introns. 1 cm = 3 kb. Dotted lines indicate the target locus for each gene. Mutant sequences are aligned to corresponding WTs. Dashes represent deleted bases. Spaces represent inserted bases. For *tmc1*, the 20 bp Cas9 target sequence (bold) and adjacent PAM sequence (underlined) are indicated. For *tmc2a*, the TALEN-deleted sequence is indicated (bold). For *tmc2b*, a G > T point mutation yields a TGA stop codon (bold). All *tmc1/2a/2b* double- and triple-mutant larvae include the $tmc1^{Ex3,\ +1bp(1)}$ allele; however, the $tmc1^{Ex3,\ +1bp(2)}$ allele also appears in *tmc1/2a* mutants used for microphonics assays. The *tmc1* single mutants are homozygous for the $tmc1^{Ex3,\ -5bp}$ allele. ***B***, The AEBR is absent in *tmc1/2a/2b* triple-mutant larvae ($n = 9$) at 5 dpf, suggesting complete deafness (WT = 70 ± 20.5%; mutant = 0 ± 0%; $t = 10.26$; df = 8.0). ***C***, **tmc1/2a/2b* triple-mutant larvae show characteristics of vestibular dysfunction. They rest on their sides or backs in a Petri dish without regard for gravitational direction, and they fail to inflate their swim bladders. A WT sibling is included for comparison. ***D***, VIEM in *tmc1/2a/2b* triple mutants at 5 dpf is lacking, further demonstrating the absence of vestibular function (WT = 1.0 ± 0.22 AU; mutant = 0.1 ± 0.057 AU; $t = 7.88$; df = 3.26).

Genotyping methods

For the *tmc1* mutant alleles and the $tmc2b^{sa8817}$ allele, we genotyped fish using kompetitive allele-specific PCR (KASP) genotyping (LGC Genomics), per the manufacturer's instructions. Briefly, KASP uses a PCR with allele-specific primers (proprietary reagents) to distinguish alleles via fluorescent labeling of PCR amplimers. Endpoint comparisons of relative fluorescence intensities of fluorophores reveal each genotype. For $tmc1^{Ex3,\ +1bp(1)}/tmc2b^{sa8817}$ mutants, either $tmc1^{Ex3,\ +1bp(1)}$ or $tmc2b^{sa8817}$ KASP serves as a proxy for the other allele due to the genes' tight linkage. The *tmc2a* genotypes were confirmed by PCR, with amplicon lengths (23 bp difference) resolved by 2.5% agarose gel electrophoresis.

When possible, mutant genotypes were determined using specific patterns of neuromast labeling, observed by fluorescence stereoscope following 30 s bath exposure to E3 containing 3 μM *N*-(3-triethylammoniumpropyl)-4-(4-(dibutylamino)styryl)pyridinium dibromide (FM 1–43, Invitrogen), which selectively labels hair cells bearing intact MET channels. As previously reported (Chou et al., 2017), only the SO1, SO3, and IO4 neuromasts label with FM 1–43 in *tmc2b* mutants, while no neuromasts label in *tmc2a/tmc2b* double mutants. Combined with knowledge of parental genotypes and relative gene crossover rates, these dye-labeling patterns facilitated identification of $tmc2b^{sa8817}$ single, $tmc2a^{Ex4,\ -23bp}/tmc2b^{sa8817}$ double, and $tmc1^{Ex3,\ +1bp(1)}/tmc2a^{Ex4,\ -23bp}/tmc2b^{sa8817}$ triple mutants. For *tmc* triple mutants carrying *Tg(myo6b:tmc2b-mEGFP-pA)*, we genotyped using $tmc2a^{Ex4,\ -23bp}$ PCR, $tmc1^{Ex3,\ +1bp(1)}$ KASP, and microscopy to identify *Tg(myo6b:tmc2b-mEGFP-pA)* by a coexpressed fluorescent heart marker, *Tg(cmlc2:mEGFP-pA)* (Kwan et al., 2007). The *tmc2b* genotype in *Tg(myo6b:tmc2b-mEGFP-pA)* larvae is reliably inferred from $tmc1^{Ex3,\ +1bp(1)}$ KASP results due to close *tmc1/2b* linkage.

Acoustic-evoked behavioral response (AEBR)

AEBR testing was conducted as previously described (Einhorn et al., 2012; Erickson et al., 2017; Maeda et al., 2017; Pacentine and Nicolson, 2019) using the Zebrabox monitoring system (ViewPoint Life Sciences). Briefly, 5 dpf mutant larvae and siblings were subjected to a 100 ms, 1 kHz pure tone at 157 decibel sound pressure level (dB SPL, relative to 1 μPa) every 15 s for 3 min. Larvae were confined, in the dark, in wells of a 96-well plate (200 μl E3/well) during the experiment. We precalibrated the wells using an underwater microphone and oscilloscope to ensure equal dB SPL exposure for all larvae. An infrared camera recorded larval movements in the dark. Zebrabox software analyzed videos for pixel changes and plotted these as movement intensity over time for each larva. Evoked responses were distinguished from background movement if they occurred within 2 s after stimulus and surpassed a defined threshold for movement intensity. We excluded individual responses from a given trial any time a larva moved within 2 s before that stimulus. For each larva, we calculated positive responses as a percentage of total responses and selected the best of three trials for inclusion in the final dataset. We calculated the mean ± SD for each genotype and used the two-tailed unpaired *t* test with Welch's correction to compare mutants to corresponding siblings, assayed simultaneously.

Vestibular-induced eye movement (VIEM)

Tests of the VIEM used the same methods, software, and devices described previously (Mo et al., 2010). In brief, 5 dpf larvae were mounted dorsally, without anesthetic, in 2% low melting point agarose on a small cover slip. Minimal excavation of agarose followed by application of an E3 droplet permitted free eye movement for immobilized larvae. Mounted larvae were positioned vertically, head down, between an infrared camera and an infrared LED array on a programmable rocking platform. Larvae were mounted off-center from the horizontal axis of rotation and kept in darkness during the experiment. The platform rocked (−45° to 45°) at 0.25 Hz frequency for 60 s while larval eye movements were video recorded in infrared.

Subsequent software-based video analyses quantified the amplitudes of angular eye movements as a function of their frequency of repetition. Larvae with normal VIEM show peak movement amplitude at 0.25 Hz, in synchrony with platform rotation. Baseline spontaneous eye movement, taken as the average amplitude across all quantified frequencies, was subtracted to determine the VIEM amplitude at 0.25 Hz. All amplitude results were normalized to the mean amplitude of WT sibling larvae assayed on the same day. We calculated the mean ± SD of each dataset

and used the two-tailed unpaired *t* test with Welch's correction to compare mutants to their corresponding siblings.

FM labeling of inner ear sensory hair cells

Direct microinjection of 2–3 nl of 0.1 M KCl with 3 μM FM 1–43 or 3 μM red-shifted N[scap]-(3-triethylammoniumpropyl)−4-(6-(4-(diethylamino)phenyl) hexatrienyl) pyridinium dibromide (FM 4-64; Invitrogen) sufficiently filled 6 dpf otic capsules to expose all inner ear hair cells to FM dye. Micropipettes were pulled from borosilicate glass capillary tubes (Sutter, item #BF150-86-10, O.D.: 1.5 mm, I.D.: 0.86 mm, fire-polished, with filament) using a Model P-97 flaming/brown micropipette puller (Sutter Instruments) and subsequently beveled using a BV-1°C micropipette beveler with impedance meter (Sutter Instruments). When filled with 0.1 M KCl and in contact with 154 mM NaCl external solution (0.9% w/v), micropipette impedance before beveling was 11–12 MΩ, and final impedance after beveling was 2–3 MΩ. Beveled micropipettes were examined via dissecting stereoscope to confirm tip quality and sharpness. Working solutions of 3 μM FM dye in 0.1 M KCl were prepared fresh from frozen FM 1–43 stock (3 mM) or FM 4–64 stock (300 μM) on the day of use, and all FM dyes were protected from light. Needles were calibrated with a slide micrometer before use and recalibrated, as needed, to ensure consistent volume delivery.

The FM dyes were not flushed from the ears to minimize hair cell damage. As a result, the hair cells were exposed to FM dye throughout the course of imaging. We made every effort to minimize experimental variability between injection days; however, multiple variables including continuous dye exposure, the tendency of FM dyes to gather in intracellular vesicles, and unavoidable variations in injection volume confound the validity of quantification sufficiently to preclude its use.

Immunohistochemistry

Immunofluorescent staining used a previously described anti-Pcdh15a monoclonal antibody and accompanying protocol (Maeda et al., 2014, 2017). WT and $tmc1^{Ex3,+1bp(1)}/tmc2a^{Ex4,-23bp}/tmc2b^{sa8817}$ triple-mutant larvae (5 dpf) were fixed overnight in PBS with 0.1% Tween-20 and 4% PFA at 4°C with nutation. Fixed larvae were then washed 3 times for 10 min at room temperature in PBST and permeabilized in PBS with 0.5% Triton X-100 for 1 h at room temperature on an orbital shaker at 50 rpm, followed by overnight permeabilization at 4°C without shaking. Larvae then shook for 2 h at room temperature in blocking buffer containing 1× PBS, 1% DMSO, 5% goat serum, and 1% BSA. Anti-Pcdh15a monoclonal antibody (1:200 in blocking buffer) was applied, incubating overnight at 4°C with nutation. Following three 15 min washes in PBST at room temperature with shaking, light-protected larvae incubated for 4–5 h at room temperature with shaking, in blocking buffer containing 1:500 dilution of AlexaFluor-546-conjugated goat anti-mouse IgG (Invitrogen) and 1:100 dilution of AlexaFluor-488-conjugated phalloidin (Invitrogen). Finally, larvae were washed 3 times for 10 min at room temperature and stored at 4°C before confocal imaging with a 63×/0.95 Achroplan water immersion objective.

Confocal microscopy

All confocal imaging used an LSM700 laser-scanning microscope (Carl Zeiss), 488 and 555 nm wavelength lasers, and Zen software (Carl Zeiss) with preprogrammed settings for fluorophore-specific emission filtering. Data collection used linear scanning, 4-sample pixel averaging, 512 × 512 pixel resolution, and 8-bit color depth. Except where specified, imaging used a 63×/0.95 Acroplan water-immersion objective and 2% laser power. Larvae were mounted laterally on a depression slide in a minimal volume of 1.2% low melting point agarose prepared in E3. All live imaging used anesthetized larvae and immersion under water containing 0.03% MESAB. Three-dimensional models of stereocilia bundles (see Fig. 2*A*) were generated using Imaris software; however, all other image processing and analysis were performed using ImageJ software.

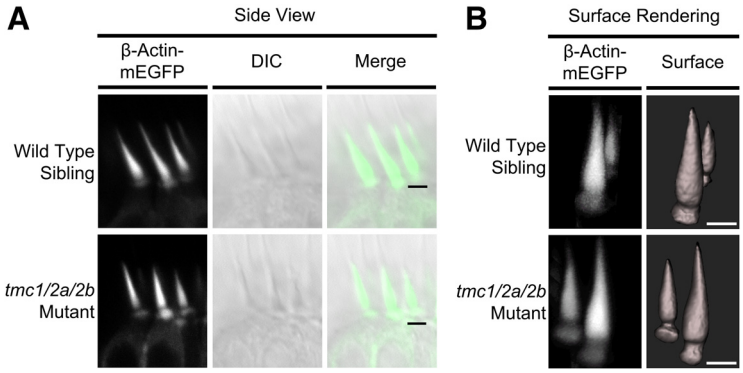

Figure 2. Gross morphology of stereociliary bundles remains intact in *tmc1/2a/2b* triple mutants. Hair cell-specific expression of *Tg(myo6b:β-Actin-mEGFP-pA)* fluorescently labels actin-filled stereocilia in *tmc1/2a/2b* triple mutants and WT siblings. ***A***, *In vivo* confocal microscopy of lateral cristae (side view) reveals no bundle splaying or other obvious defects of bundle morphology in *tmc1/2a/2b* triple-mutant larvae (5 dpf). Scale bar, 2.5 μm. ***B***, Three-dimensional surface rendering of confocal *z* stacks demonstrates two distinct bundle height groups in centrally located mature hair cells, regardless of genotype. These bundle heights correspond to two hair-cell types in the cristae. Fluorescent patches at the base of bundles are labeling of actin filaments in the cuticular plate. Scale bar, 2 μm.

Fluorescent signal quantification

Levels of Pcdh15a, mEGFP-Lhfpl5a, and Tmie-mEGFP protein localization (see Fig. 3) were quantified as described previously (Pacentine and Nicolson, 2019). Using ImageJ, we generated maximum projections from *z*-stack images of the middle cristae, and then outlined the region above the soma where the stereocilia reside as the ROI. Within the ROI, we quantified the integrated density of the channel with an emission peak at 480 nm. We used 5-slice projections for anti-Pcdh15a, 15-slice projections for mEGFP-Lhfpl5a, and 18-slice projections for Tmie-mEGFP. To subtract background signal, we used an ROI drawn above the stereocilia. We calculated the mean ± SD of each dataset and compared mutants to corresponding siblings using the two-tailed unpaired *t* test with Welch's correction.

Microphonics

Microphonics measurements were collected and analyzed as previously described (Pacentine and Nicolson, 2019). We anesthetized 3 dpf larvae with 0.02% MESAB in extracellular solution containing 140 mM NaCl, 2 mM KCl, 2 mM $CaCl_2$, 1 mM $MgCl_2$, and 10 mM HEPES, pH 7.4. Larvae were immobilized using glass fibers and positioned with a piezo-driven mechanical stimulation rod in light contact with the front of the head behind the lower eye, level with the otoliths of the ear of interest. The tip of a recording micropipette was inserted into the inner ear to record extracellular potentials. We used multiple-step stimuli with piezo actuator driving voltages of 2, 3, 4, 5, 6, and 10 V. Each stimulus was 20 ms in duration, with 20 ms prestimulus and poststimulus periods.

For each larva, we recorded 200 traces at 20 kHz and generated an average trace response. We then measured the baseline-to-peak amplitude for each average trace. To identify statistically significant differences between genotypes across the step stimulus driving voltages (see Figs. 4*A*, 5*B*), we used two-way ANOVA to compare all groups within a larval clutch. To compare *tmc* single and double mutants (see Fig. 7*A*), we used data collected at the strongest driver stimulus (10 V) and normalized to the mean amplitude of the corresponding WT siblings. Then we calculated the normalized mean ± SD for each genotype and used the two-tailed unpaired *t* test with Welch's correction to identify statistically significant differences between mutant genotypes and their WT siblings.

Experimental design and statistical analyses

All experiments use larvae 3–6 dpf, after the onset of MET activity and before larvae require feeding. Gender differentiates later in development and does not factor into the experimental design. AEBR, VIEM,

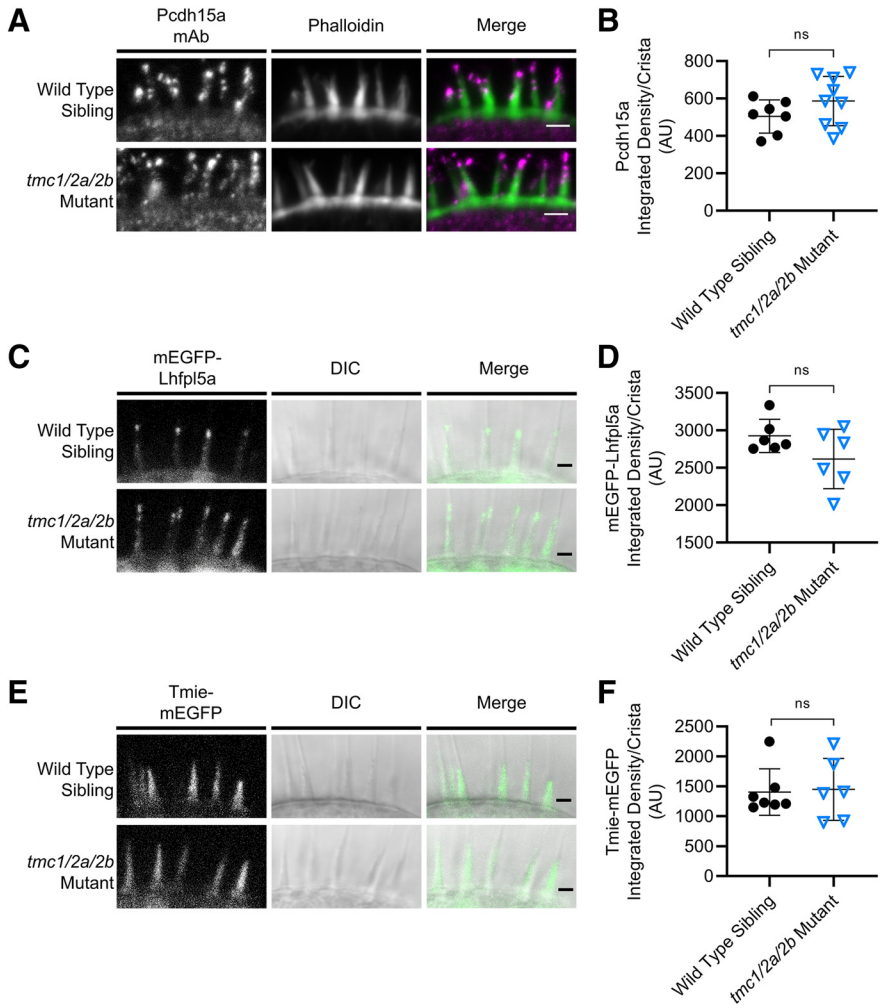

Figure 3. MET components are unaffected in the inner ear (cristae) of *tmc1/2a/2b* triple mutants (5 dpf). ***A***, Immunohistochemistry shows comparable localization of Pcdh15a (magenta in merge panel) at the tips of stereocilia (green) in *tmc1/2a/2b* triple mutants. Scale bar, 2 μm. ***C***, ***E***, *In vivo* fluorescence imaging similarly reveals similar patterns of localization of mEGFP-Lhfpl5a (***C***) or Tmie-mEGFP (***E***). Scale bar, 2 μm. ***B***, ***D***, ***F***, Quantification of fluorescence shows no significant differences in expression levels of all three proteins relative to WT levels (ns indicates $p > 0.1$). ***B***, WT = 504 ± 88.7 AU; mutant = 587 ± 132 AU; $t = 1.49$; df = 13.79. ***D***, WT = 2927 ± 222 AU; mutant = 2618 ± 132; $t = 1.66$; df = 7.86. ***F***, WT = 1404 ± 388; mutant = 1449 ± 518; $t = 0.175$; df = 9.2.

immunohistochemistry, and live fluorescence confocal imaging use 5–6 dpf larvae for consistency of results and because WT larvae at this stage have sufficient numbers of mature hair cells with intact MET channels to detect and respond to auditory/vestibular input. For microphonics recordings, we use 3 dpf larvae because the otic capsule is softer, which facilitates insertion of, and prevents damage to, the recording micropipette.

For all experiments subject to statistical analyses, we used G*power software (Faul et al., 2007) for *a priori* calculations of minimum sample sizes necessary to achieve acceptable levels of statistical power. We conducted all other statistical analyses using GraphPad Prism 8 software. Microphonics results were analyzed using two-way ANOVA to calculate *p* values reported in Figures 4*A* and 5*B*. We used the two-tailed unpaired *t* test with Welch's correction for AEBR, VIEM, fluorescence signal quantification analyses (see Fig. 3), and microphonic potential comparisons at 10 V (see Fig. 7*A*). In all cases, exact *p* values are reported, except when $p > 0.1$ or $p < 0.0001$.

Results

tmc1/2a/2b triple-mutant zebrafish larvae do not respond to acoustic or vestibular stimuli

The *tmc1*, *tmc2a*, and *tmc2b* genes are located on chromosome 5, with the loci of *tmc1* and *tmc2b* in close proximity. We used a combination of crossing and genetic editing methods to produce a line carrying the $tmc1^{Ex3,\ +1bp(1)}$, $tmc2a^{Ex4,\ -23bp}$, and $tmc2b^{sa8817}$ alleles (Fig. 1*A*; for details, see Materials and Methods). Upon successful generation of the *tmc1/2a/2b* triple-mutant line, we tested gross behavioral responses to acoustic and vestibular stimuli (Fig. 1*B–D*).

We examined the AEBR in larvae to quantify behavioral responses to auditory stimuli. The experiments revealed that the *tmc* triple mutants do not startle in response to auditory stimuli at high sound pressure levels, suggesting that they are completely deaf (Fig. 1*B*). At rest in a Petri dish, the *tmc* triple mutants make no effort to maintain an upright floating posture relative to gravity (Fig. 1*C*). Instead, they rest on their sides or backs at the bottom of the dish, which is a characteristic feature of vestibular defects in fish. The *tmc* triple mutants also fail to inflate their swim bladders, as they do not swim to the water's surface to take in air. Upon direct prodding with a dissection needle, *tmc* triple mutants attempt to swim; however, they do so at random pitch and roll orientations, disregarding the direction of gravitational force. To test vestibular function, we measured VIEM. Results from *tmc* triple mutants (Fig. 1*D*) showed no reflexive eye movements above background levels in response to a combination of linear and angular momentum, confirming the absence of vestibular function. These tests suggest that *tmc1/2a/2b* triple mutants are deaf and incapable of detecting vestibular cues.

Disruption of *tmc1/2a/2b* does not affect hair-bundle morphology or trafficking of other MET channel components

Given the critical role of Tmc1/2a/2b in MET and known binding interactions with other proteins of the MET channel, we examined hair-bundle morphology and the localization of other known MET components in *tmc1/2a/2b* triple-mutant larvae. We visualized stereocilia in *tmc* triple mutants and their WT siblings using *Tg(myo6b:β-actin-mEGFP-pA)*. We compared hair-bundle morphology *in vivo* using fluorescent and differential interference contrast confocal microscopy. The gross structure of hair bundles was comparable between *tmc* triple mutants and WT siblings (Fig. 2*A*).

Three-dimensional modeling of the bundle-filling β-Actin-mEGFP label (Fig. 2*B*) revealed no obvious differences in bundle dimensions between *tmc* triple mutants and their WT siblings. Hair bundles showed no signs of splaying, in agreement with previous findings using Tomt-deficient or Tmie-deficient fish presumed to mimic a *tmc* triple-mutant phenotype (Erickson

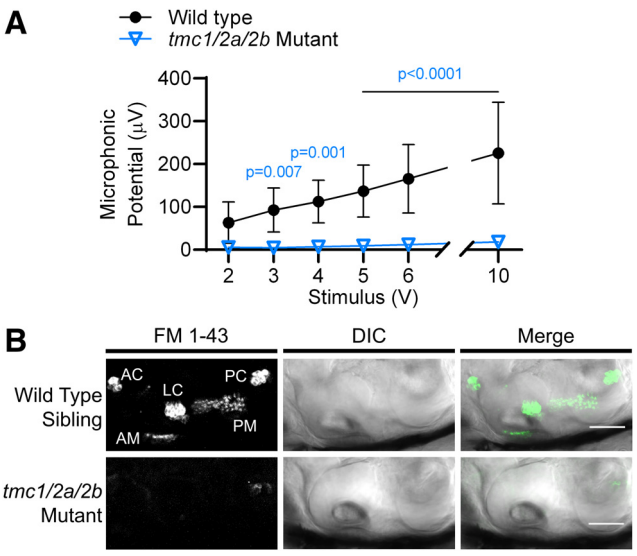

Figure 4. Hair cells in *tmc1/2a/2b* triple mutants lack mechanosensitivity. ***A***, The amplitude of microphonic potentials correlates with stimulus intensity in WT siblings; however, *tmc1/2a/2b* triple-mutant larvae (3 dpf) have no detectable microphonic potentials, even with high-intensity stimuli ($n = 9$ for each genotype; $F_{(1,16)} = 32.3$). ***B***, Otocyst injection of FM 1-43 vital dye, which labels hair cells with intact MET channels, does not label inner ear hair cells in *tmc1/2a/2b* triple-mutant larvae (6 dpf), further demonstrating a uniform lack of hair-cell activity in all end organs. Side view of inner ear is shown. *Injection damage. AC, Anterior crista; LC, lateral crista; PC, posterior crista; AM, anterior macula; PM, posterior macula. Scale bar, 50 μm.

et al., 2017; Pacentine and Nicolson, 2019). The modeling did, however, reveal two distinct bundle types (tall and short), which correspond to two distinct cell body morphologies in the lateral cristae of all larvae, independent of *tmc1/2a/2b* disruption (Fig. 2*B*).

To identify consequences of loss of Tmc proteins on localization of other known MET components, we compared expression patterns of Pcdh15a, Lhfpl5a, and Tmie in *tmc1/2a/2b* triple-mutant and WT sibling larvae. Immunohistochemistry results showed no differences in localization (Fig. 3*A*) or significant changes in the amount (Fig. 3*B*) of anti-Pcdh15a labeling in hair bundles. *In vivo* imaging of *tmc* triple mutants and WT siblings that express either of the transgenes *Tg(myo6b:mEGFP-lhfpl5a-pA)* or *Tg(myo6b:tmie-mEGFP-pA)* also showed no significant changes in the localization patterns or amounts of mEGFP-Lhfpl5a (Fig. 3*C*,*D*) or Tmie-mEGFP (Fig. 3*E*,*F*). Together, these results suggest that hair bundles are intact and central components of the MET complex are properly localized in *tmc* triple mutants.

tmc1/2a/2b triple mutation eliminates hair-cell activity

When both TMC1 and TMC2 are knocked out in mice, MET currents in auditory/vestibular hair cells are absent (Kawashima et al., 2011). Likewise, loss of two Tmcs (Tmc2a/2b) results in complete loss of activity in lateral-line and posterior macular hair cells of zebrafish (Chou et al., 2017; Chen et al., 2020). To test hair-cell activity in the zebrafish inner ear, we used two methods: recordings of extracellular microphonic potentials and labeling by the vital dye FM 1-43. Previous reports of microphonic recordings in zebrafish suggest that most of the signal detected from inner ear recordings is generated by the maculae, predominately the posterior macula (Lu and DeSmidt, 2013). The posterior macula develops into the saccule, the hearing organ of zebrafish. To test the activity of the inner ear maculae, we recorded extracellular microphonic potentials from inner ear hair cells in *tmc* triple mutants. In WT siblings, the amplitude of microphonic potentials of the inner ear correlated with stimulus intensity; however, the same stimuli evoked no detectable microphonic potentials in *tmc* triple mutants (Fig. 4*A*).

To verify the absence of hair-cell activity, we injected FM 1-43 dye into the inner ears of *tmc* triple-mutant and WT sibling larvae at 5–6 dpf. FM 1–43 is a vital dye that enters hair cells via MET channels (Gale et al., 2001) and fails to label zebrafish hair cells with MET defects (Seiler and Nicolson, 1999). In WT larvae, FM 1–43 labeled macular hair cells as well as hair cells of the three cristae, which develop into the ampullae of the semicircular canals. By contrast, no cells were labeled in *tmc* triple mutants (Fig. 4*B*). Collectively, the data from our microphonic recordings and FM labeling confirm the uniform absence of MET function in the *tmc* triple mutants.

Tg(myo6b:tmc2b-mEGFP-pA) rescues hair-cell activity in *tmc1/2a/2b* triple-mutant larvae

Our results suggest that the *tmc* triple-mutant larvae completely lack MET channel activity while maintaining expression of other major MET components; consequently, we attempted to rescue MET in *tmc* triple mutants using expression of transgenes. Because of technical reasons, we were unable to express Tmc1-mEGFP and Tmc2a-mEGFP (see Materials and Methods). Fluorescence imaging of Tmc2b-mEGFP in lateral cristae demonstrated proper localization to the stereocilia bundles in each larva (Fig. 5*A*), as previously reported (Erickson et al., 2017; Pacentine and Nicolson, 2019). Although we directly confirmed proper localization in lateral cristae, bundle localization of Tmc2b-mEGFP was difficult to visualize at the same developmental stage in the corresponding maculae due to the depth of these structures in the otocyst. Nevertheless, Tmc2b-mEGFP and FM 4-64 were detectable in the macular hair-cell bodies, implying bundle localization (Figs. 5*C*, 6*C*).

Tmc2b-mEGFP expression was sufficient to restore vestibular function in *tmc* triple-mutant larvae (Fig. 5). VIEM in *tmc* triple mutants was rescued to levels similar to WT siblings (Fig. 5*B*). In addition, FM labeling of hair cells was restored in the *tmc1/2a/2b* triple-mutant cristae and anterior maculae, with a similar appearance to WT siblings (Fig. 5*A*,*C*).

Tmc2b-mEGFP also rescued hair cell function in the auditory system (Fig. 6). Although the AEBR data indicated variable levels of rescue (Fig. 6*A*), the difference was not significantly different from WT siblings. Previous reports have found that behavior can be rescued without full rescue of hair-cell activity as measured by more direct methods (Erickson et al., 2017; Pacentine and Nicolson, 2019), so we also compared hair-cell activity in WT siblings and *tmc* triple-mutant larvae expressing Tmc2b-mEGFP. Hair-cell activity in the auditory system was rescued to WT levels by expression of the Tmc2b-mEGFP transgene, as demonstrated by both microphonic recordings (Fig. 6*B*) and labeling by FM dye in the posterior maculae (Figs. 5*C*, 6*C*).

Posterior macular hair cells rely primarily on *tmc2a* and *tmc2b* with minimal contribution from *tmc1*

The results described above (1) confirm the expectation that concurrent disruption of *tmc1/2a/2b* leads to complete loss of MET activity and (2) reveal that exogenous Tmc2b-mEGFP can rescue auditory/vestibular deficits and restore FM labeling in all mechanosensory end organs. We noted, however, that triple mutants were distinguishable from double mutants at 5 dpf, suggesting some differences in the reliance on Tmc subunits. Generally,

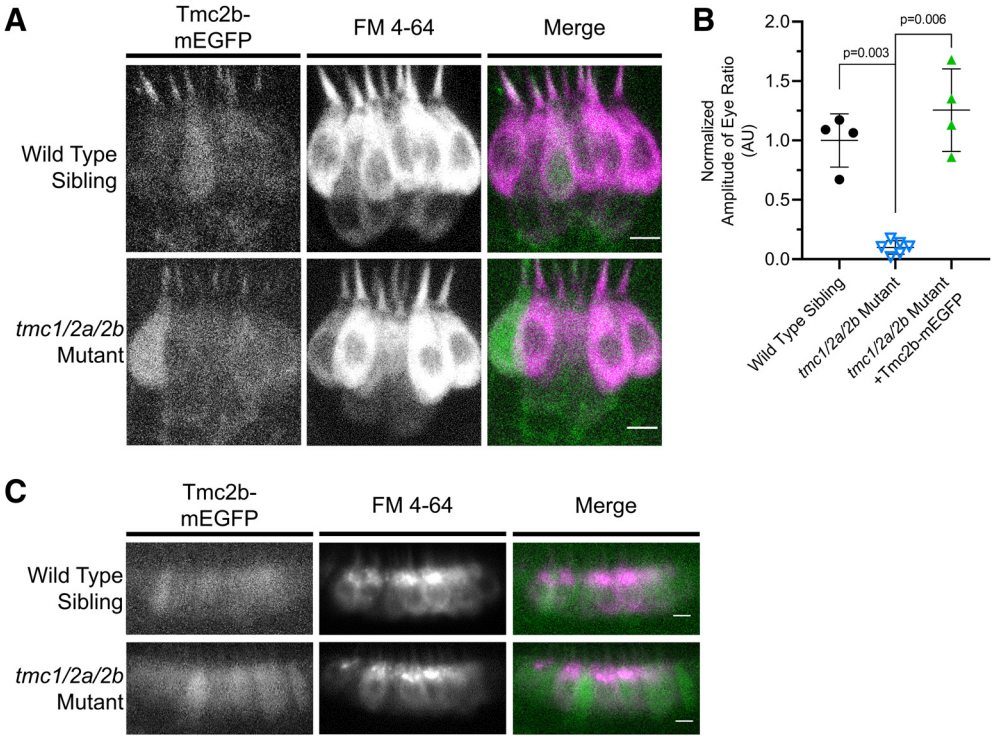

Figure 5. *Tg(myo6b:tmc2b-mEGFP-pA)* expression rescues vestibular function in *tmc1/2a/2b* triple-mutant larvae (5 dpf). ***A***, Side view of lateral cristae. Tmc2b-mEGFP localizes to hair bundles and rescues FM 4-64 hair-cell labeling in the *tmc1/2a/2b* triple mutants (WT, $n = 7$; mutant, $n = 8$). Scale bar, 5 μm. ***B***, Tmc2b-mEGFP rescues the VIEM deficit in *tmc1/2a/2b* triple mutants (mutant = 0.099 $\pm$ .0.057 AU; mutant with transgene = 1.26 $\pm$ 0.35 AU; $t = 6.6$; df = 3.1). ***C***, Tmc2b-mEGFP rescues FM 4-64 hair-cell labeling in mutant *tmc1/2a/2b* anterior maculae (side view) (WT, $n = 7$; mutant, $n = 7$). Scale bar, 5 μm.

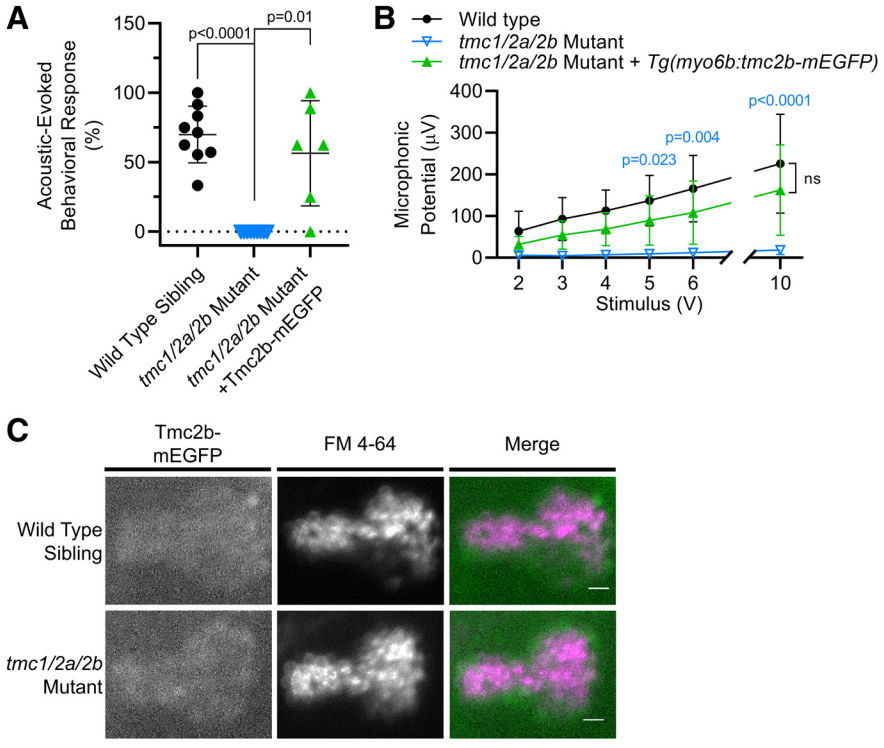

Figure 6. *Tg(myo6b:tmc2b-mEGFP-pA)* expression rescues hearing in *tmc1/2a/2b* triple-mutant larvae (5 dpf). ***A***, The AEBR deficit is rescued by Tmc2b-mEGFP in *tmc1/2a/2b* triple-mutant larvae (mutant = 0 $\pm$ 0%; mutant with transgene = 56.5 $\pm$ 37.9%; $t = 3.65$; df = 5.0). ***B***, Tmc2b-mEGFP restores microphonic potentials in *tmc1/2a/2b* triple mutants ($n = 8$ rescued larvae; $n = 9$ for other genotypes; $F_{(2,23)} = 14.68$). *p* values (blue) compare *tmc1/2a/2b* triple mutants with and without *Tg(myo6b:tmc2b-mEGFP-pA)*. ***C***, Tmc2b-mEGFP restores FM 4-64 labeling of hair cells in the posterior maculae (top down view) of *tmc1/2a/2b* triple mutants (WT, $n = 5$; mutant, $n = 5$). Scale bar, 10 μm.

double mutants responded on occasion to tapping on the Petri dish or could partially orient to gravity. Therefore, we characterized the phenotypes of *tmc* single- and double-mutant larvae to determine the relative contributions of each gene to MET activity in different hair-cell subpopulations.

To assess hair-cell activity in the maculae, we recorded microphonics and AEBR from *tmc* single and double mutants (Fig. 7), which further elucidated details of the division of roles among the Tmcs. Interestingly, the *tmc2a* single mutants ($n = 8$) had significantly reduced microphonic signals compared with WT siblings ($n = 7$) and were the only single-gene mutants with such a deficit ($p = 0.001$; $t = 4.34$; df = 8.36) (Fig. 7*A*). When combined with the *tmc1* allele, the *tmc1/2a* double mutants showed no further reduction in microphonic signal compared with the *tmc2a* single mutant. These results suggest that Tmc1 does not have a biologically relevant effect on hair-cell activity in the macular end organs.

Consistent with the *tmc2a* deficit, the amplitude of microphonic signals from *tmc2b* single mutants, *tmc1* single mutants, and *tmc1/2b* double mutants was comparable to WT siblings (Fig.

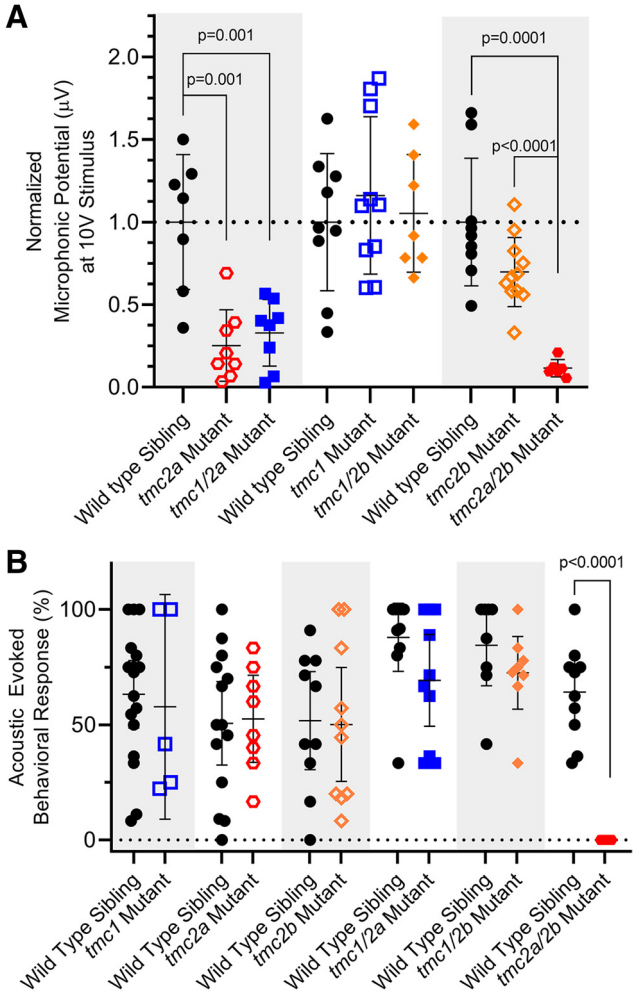

Figure 7. Detection of sound by single and double *tmc1/2a/2b* mutants (5 dpf). Shaded areas in graphs group each mutant genotype with its corresponding siblings. ***A***, Microphonic potentials are significantly reduced in larvae carrying the *tmc2a* allele (single or double mutants), with the greatest reduction in *tmc2a/2b* double-mutant larvae. Normalized amplitudes using 10 V stimulus are shown. For *tmc2a* and *tmc1/2a*, WT = 1.0 ± 0.41 μV; *tmc2a* = 0.25 ± 0.22 μV; *tmc1/2a* = 0.33 ± 0.2 μV. Compared with WT, *tmc2a* $t = 4.34$; df = 8.36 and *tmc1/2a* $t = 3.94$; df = 8.48. For *tmc2a/2b*, WT = 1.0 ± 0.39 μV; *tmc2a/2b* = 0.12 ± 0.05 μV; $t = 6.77$; df = 8.43. ***B***, Concurrent mutation of *tmc2a/2b* is sufficient and necessary to eliminate AEBR relative to corresponding WT siblings (WT = 64.2 ± 20.6%; *tmc 2a/2b* mutant = 0 ± 0%; $t = 9.86$; df = 9.0).

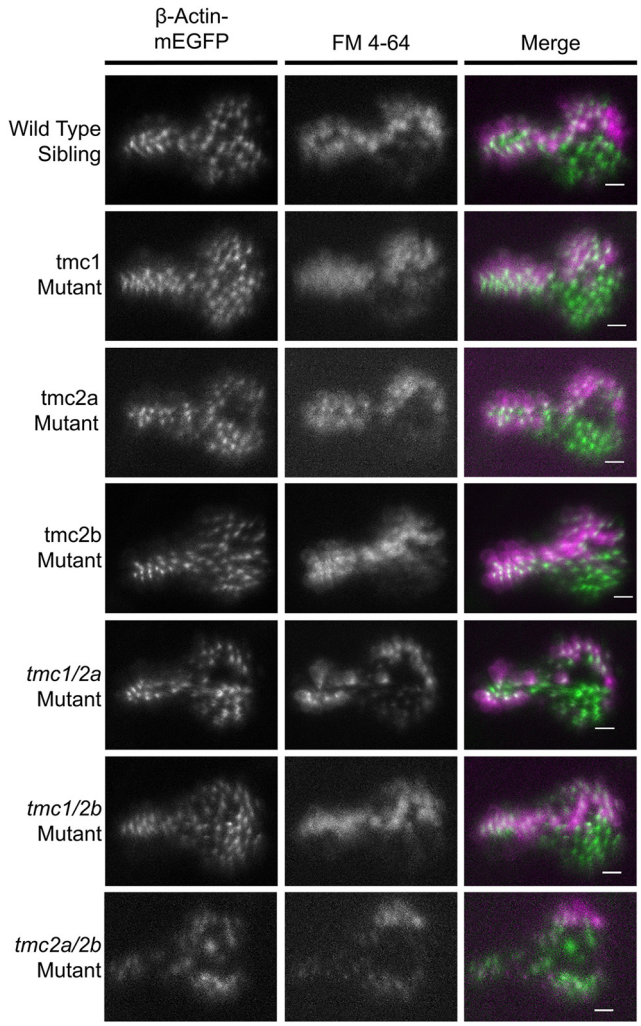

Figure 8. FM labeling of the posterior macula in single and double *tmc1/2a/2b* mutants (5 dpf). Otocysts of *Tg(myo6b:β-Actin-mEGFP-pA)* larvae of each genotype were injected with FM 4-64 vital dye. Representative top down views of the posterior macula are shown. GFP-positive hair bundles (green) were overlaid with FM 4-64 label (magenta) in the merge panels. *tmc2a/2b* double mutants show the strongest reduction in FM 4-64 label throughout the neuroepithelium, with the exception of a subset of hair cells at the periphery of the dorsal posterior region. We examined multiple specimens per genotype (WT, $n = 8$; *tmc1*, $n = 8$; *tmc2a*, $n = 7$; *tmc2b*, $n = 5$; *tmc1/2a*, $n = 7$; *tmc1/2b*, $n = 5$; *tmc2a/2b*, $n = 5$). Scale bar, 10 μm.

7*A*). These results suggest that Tmc2a, on its own, is sufficient for MET function in the maculae. While *tmc2b* single mutants do not have a significant reduction in microphonic potentials, the reduction in *tmc2a/2b* double mutants ($p = 0.0001$; $n = 6$; $t = 6.77$; df = 8.43) is more severe than when *tmc2a* alone is disrupted (Fig. 7*A*). These results suggest that Tmc2b makes some contribution to macular hair-cell activity.

We next assessed whether the reduced hair-cell activity of *tmc* single and double *tmc* mutants had an impact on behavioral reflexes. With regard to AEBR, only one genotype yielded a statistically significant difference: the *tmc2a/2b* double mutants ($p > 0.0001$; $n_{WT} = 10$; $n_{tmc2a/2b} = 6$; $t = 9.86$; df = 9.0) (Fig. 7*B*). These larvae, retaining only Tmc1 function, never responded to sound in this assay, similar to the triple mutants. This result demonstrates that Tmc1 is insufficient on its own and has a negligible contribution to hearing in zebrafish larvae. We postulate that Tmc2a and Tmc2b must both contribute to MET activity in the posterior macula/saccule because no other single- or double-mutant genotypes caused a significant reduction in AEBR. Our data also suggest that Tmc2a and Tmc2b are each sufficient on their own to enable the detection of sound, although the microphonics data suggest that loss of Tmc2a has a stronger effect on hair-cell activity.

The microphonic recordings and AEBR experiments reflect population-level activity. To test for qualitative differences in Tmc-dependent activity in individual hair cells within the posterior macula, we injected FM 4-64 dye into the inner ears of single and double mutants (Fig. 8). In these experiments, the mutants also expressed transgenic β-actin-mEGFP, which enabled the visualization of the shape and boundaries of the posterior macula. Unlike in other end organs, we noted small gaps in the β-actin-mEGFP labeling in the central region of the posterior macula in larvae carrying the $tmc2a^{Ex\ 4,\ -23bp}$ allele in any combination. The reason for the gap in the central neuroepithelium is not clear. Expression of the *tmc2b* transgene appears to mitigate this effect (Fig. 5*C*).

In keeping with the other experiments, the *tmc2a/2b* double mutants showed the most obvious loss of FM 4–64 labeling, as only hair cells on the boundary of the posterior macula's larger lobe had detectable FM label (Fig. 8). This reduction in FM 4–64 labeling showed that, while Tmc1 provides little overall contribution to behavior and population-level hair-cell activity, it is sufficient for MET function in a small subset of saccular hair cells. Also bolstering AEBR and microphonics results, *tmc2a* and *tmc1/2a* mutants had patterns of reduced FM labeling similar to each other but distinct from other genotypes. In contrast, the *tmc1/2b* single and double mutants had FM labeling patterns similar to WT siblings. Together, these results demonstrate a Tmc2a > Tmc2b > Tmc1 hierarchy in the detection of sound.

Anterior macular hair cells rely primarily on *tmc2b*, with secondary contributions from *tmc2a* and *tmc1*

With regard to vestibular function of the utricle/anterior macula, we observed a reduction in VIEM in both *tmc1/2b* and *tmc2a/2b* double mutants, whereas all other genotypes yielded responses that were not statistically different from their siblings (Fig. 9*A*). Unlike the AEBR tests, VIEM data for *tmc1/2b* double mutants in utricular function did reveal a statistically significant reduction in VIEM in this genotype ($p = 0.006$; $n_{WT} = 5$; $n_{tmc1/2b} = 13$; $t = 4.4$; df = 5.3). The two double-mutant combinations that gave rise to a deficit included the *tmc2b*^{sa8817} allele, suggesting that Tmc2b is the primary contributor to vestibular end organ function.

In addition, FM labeling of the anterior macula yielded similar deficits with respect to genotype (Fig. 9*B*). The most apparent loss of FM labeling appeared in the *tmc2a/2b* double mutant, whereas *tmc1/2b* double mutants still had noticeable, yet possibly reduced, FM labeling. Results from single mutants revealed no obvious reduction in FM labeling. Together, these results suggest a Tmc2b > Tmc2a > Tmc1 hierarchy in vestibular function.

Developing cristae contain two distinct types of hair cells with differences in *tmc1/2a/2b* dependency

We next examined hair cells in the lateral cristae, which is the most suitable end organ for *in vivo* imaging due to access and angle. Confocal microscopy of the FM labeling patterns at high magnification revealed two distinct types of hair cells in these end organs (Fig. 10). In WT siblings, individual hair cells in a single larva showed variable intensities of FM labeling, as seen in other reports (Seiler and Nicolson, 1999; Erickson et al., 2017). We found that hair cells with a teardrop shape were positioned exclusively in the upper layer of the neuroepithelium and tended to label more intensely with FM dye than the hair cells in the lower layer, which had a gourd-like shape. In addition to differences in FM labeling, our 3D modeling of bundle morphologies in lateral cristae expressing β-actin-mEGFP (Fig. 2*B*) revealed two distinct categories of bundle heights that correspond to the two hair cell types, where teardrop cells have taller stereocilia bundles and gourd cells have shorter bundles.

To determine whether the Tmc proteins had differential effects in these two hair-cell subtypes, we examined patterns of FM expression in *tmc* single and double *tmc* mutants (Fig. 10). In all KOs lacking Tmc2a (*tmc2a* mutants, *tmc1/2a* double mutants, and *tmc2a/2b* double mutants), we observed a striking loss of FM label in the teardrop cells, whereas labeling remained in the gourd-shaped cells (Fig. 10). The defect in FM labeling and reduced microphonics in the *tmc2a* mutant indicates that neither the *tmc2b* gene duplicate nor *tmc1* can compensate for the loss of *tmc2a* in this cell type. These results also demonstrate

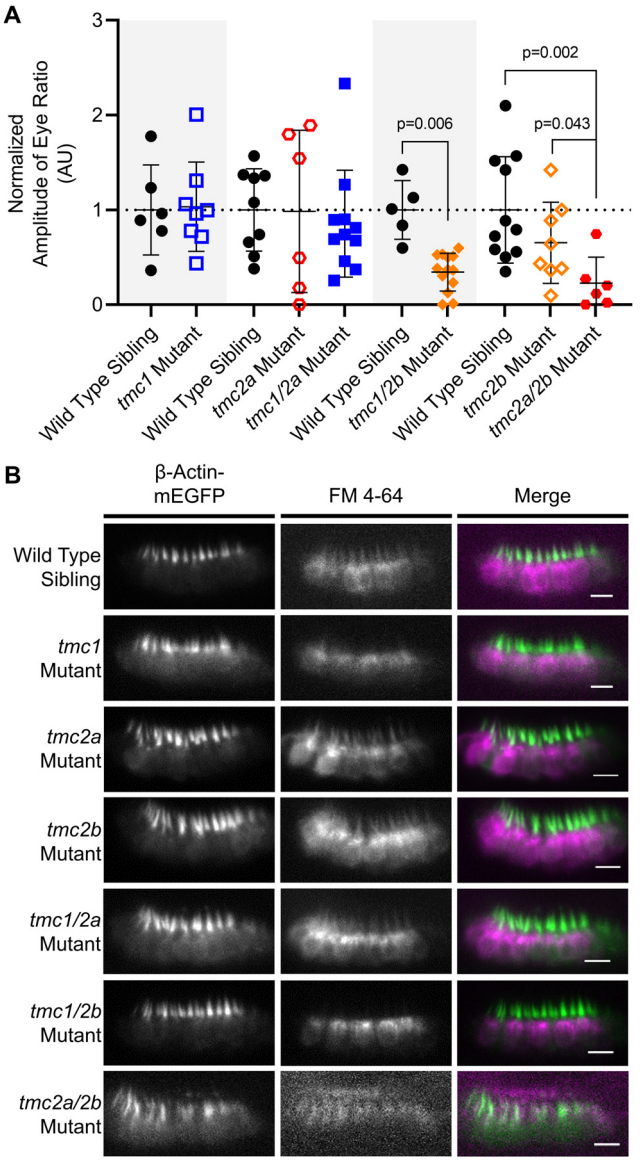

Figure 9. Vestibular function in single and double *tmc1/2a/2b* mutants (5 dpf). Gray shading represents cohorts of siblings. ***A***, Normalized VIEM in single and double mutants. For *tmc1/2b* comparison, WT = 1.0 ± 0.31 AU; *tmc1/2b* = 0.34 ± 0.20 AU; $t = 4.4$; df = 5.3. For *tmc2a/2b*, WT = 1.0 ± 0.56 AU; *2a/2b* = 0.23 ± 0.27 AU. ***B***, Confocal images of hair-cell labeling in the anterior macula (side view) of FM 4-64-injected larvae in the *Tg(myo6b:β-Actin-mEGFP-pA)* background. GFP-positive hair bundles (green) were overlaid with FM 4-64 label (magenta) in the merge panels. The *tmc2a/2b* double-mutant larvae show a loss of FM 4-64 hair-cell labeling relative to all other genotypes (background signal is associated with the otolithic membrane). We examined multiple specimens per genotype (WT, $n = 8$; *tmc1*, $n = 7$; *tmc2a*, $n = 5$; *tmc2b*, $n = 5$; *tmc1/2a*, $n = 6$; *tmc1/2b*, $n = 5$; *tmc2a/2b*, $n = 5$). Scale bar, 10 μm.

that Tmc1 and Tmc2b are each individually sufficient for MET function in the gourd cells. Consistent with these findings, combined disruption of *tmc1/2b* showed no FM label in the lower gourd cells (Fig. 10). Together, our experiments reveal that, in cristae, hair cells stratify into an upper, Tmc2a-dependent layer of teardrop-shaped cells, and a lower, Tmc1/2b-dependent tier of gourd-shaped cells.

Discussion

In the present study, we show that *tmc1/2a/2b* triple-mutant larvae lack the ability to hear or orient to gravity, indicating that

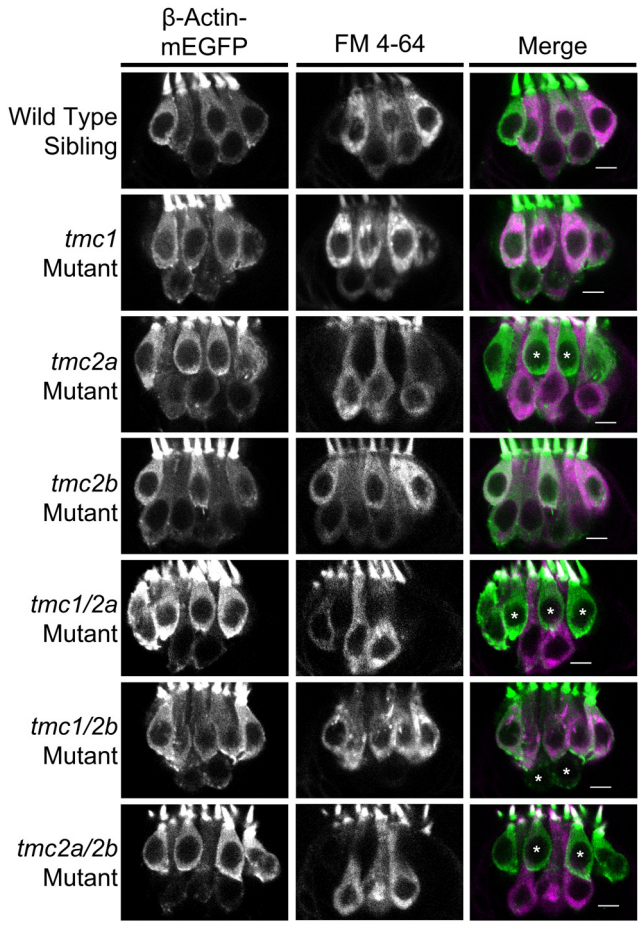

Figure 10. *tmc1/2a/2b* single and double mutants reveal molecular differences between two morphologically distinct hair-cell types in lateral cristae (5 dpf). Otocysts of *Tg (myo6b:β-Actin-mEGFP-pA)* larvae of each genotype were injected with FM 4-64 vital dye. GFP-positive hair bundles (green) were overlaid with FM 4-64 label (magenta) in the merge panels. Type I-like "teardrop"-shaped cells are located in the upper layer, whereas Type II-like, "gourd"-shaped cells are present in the lower layer of the neuroepithelium. *Centrally located mature hair cells that lack FM labeling. We examined multiple specimens per genotype (WT, $n = 8$; *tmc1*, $n = 7$; *tmc2a*, $n = 7$; *tmc2b*, $n = 5$; *tmc1/2a*, $n = 10$; *tmc1/2b*, $n = 5$; *tmc2a/2b*, $n = 7$). Scale bar, 5 μm.

these mutant alleles are functional nulls. The presence of normal hair bundle morphologies (Fig. 2) and unchanged localization patterns of other MET channel components in *tmc* triple-mutant larvae (Fig. 3), combined with absent microphonic signals and FM labeling (Fig. 4), confirm that the *tmc* triple-mutant phenotype is a direct consequence of *tmc* disruption rather than bundle splaying or abnormal protein trafficking. The inner ear phenotype of the zebrafish *tmc* triple mutants is similar to the phenotypic consequences of loss of both *Tmc1* and *Tmc2* function in the mouse inner ear (Kawashima et al., 2011, 2015). Both vestibular and auditory function are abolished and MET is absent in hair cells of double KO mice. The phenotypic similarities demonstrate the cross-species importance of the TMC1/2 proteins to MET in auditory/vestibular hair cells.

While the *tmc* triple mutants confirmed the universal role of the Tmc1/2 protein family in inner ear function, the analyses of *tmc* single- and double-mutant phenotypes uncovered important differences in Tmc1/2a/2b dependency among different groups of hair cells (Figs. 7-9). These data reveal that Tmc2a plays a key role in hearing with a Tmc2a > Tmc2b hierarchy of contribution to MET activity in the posterior macula, with little to no contribution from Tmc1. Our data reinforce the notion that Tmc1 is dispensable for hearing in zebrafish larvae, as recently reported by Chen et al. (2020). With regard to vestibular function, the major contributor is Tmc2b. In the anterior macula, a Tmc2b > Tmc2a > Tmc1 hierarchy is in play. Thus, macular hair cells in zebrafish larvae rely mainly on Tmc2a and Tmc2b to provide MET activity, and Tmc1 is a minor component that contributes to the sense of balance, but not to hearing in larvae. This scenario reflects the similarity of MET requirements in lateral line hair cells, which primarily depend on Tmc2b (Chou et al., 2017). In contrast, vestibular hair cells in mammals can function with either TMC1 or TMC2, but mature cochlear hair cells require TMC1 for MET activity (Kawashima et al., 2011; Asai et al., 2018; Nakanishi et al., 2018). Our findings suggest that, during the evolutionary development of hearing, there was a molecular switch between expression and use of the Tmc1/2 proteins.

In mature macular and ampullary end organs of fish, two or more types of hair cells have been identified based on morphologic and RNAseq criteria (Popper, 1977, 2000; Sugihara and Furukawa, 1989; Barta et al., 2018). Unlike other vertebrates, vestibular hair cells in fish are not innervated by an afferent calyx that envelopes the soma; however, evidence for calyx-like afferent structures and other morphologic features of Type I and Type II vestibular hair, cells such as variations in hair bundle architecture, has been previously reported (Popper, 1977; Lanford and Popper, 1996). Here we present genetic evidence that two morphologically distinct types of hair cells in the developing cristae display clear differences in reliance on Tmc1/2a/2b. Teardrop cells with taller stereocilia bundles with some resemblance to Type I hair cells require Tmc2a for MET activity, whereas Type II-like gourd cells with shorter bundles have Tmc2a-independent MET activity. In addition, we observe consistent differences in FM label intensities between teardrop- and gourd-shaped cells residing in the same crista (Fig. 10).

Prior studies have shown that the cation permeability and conductance properties of MET channels are affected by differences in TMC1/2 content in mice (Pan et al., 2013; Beurg et al., 2014, 2015a,b; Corns et al., 2016). Because Tmc2a-dependent teardrop cells acquire more robust FM labeling than Tmc2a-independent gourd cells, we suspect that the differences in Tmc1/2a/2b usage alter the cation permeability and/or conductance in each cell type. The differences in teardrop- and gourd-shaped cells suggest the possibility of different roles for the two cell types in a more complex and finely tuned mechanism of balance than was previously thought.

Interestingly, these two vestibular subtypes appear to be specific to the larval cristae. Only one hair cell type, resembling a single layer of teardrop cells, is evident in the larval anterior macula. In contrast to the anterior macula, which becomes functional at 3 dpf (Easter and Nicola, 1997; Mo et al., 2010), stimulation of the cristae does not produce vestibular-induced eye reflexes at larval stages (Beck et al., 2004; Mo et al., 2010). The contributions of each cell type within the semicircular canals at more mature stages are not clear, but we speculate that the teardrop and gourd cells may improve the dynamic range or otherwise modify the sensitivity of the mature vestibular system. A similar consequence on MET activity is possible in the posterior macula, where FM labeling of subsets of hair cells in *tmc* double mutants suggests differences in Tmc1/2a/2b reliance. Together, our findings provide molecular evidence of subtypes of hair cells within the same end organ of zebrafish that can be differentiated by their requirements for specific combinations of Tmc1/2a/2b subunits.

References

Asai Y, Pan B, Nist-Lund C, Galvin A, Lukashkin AN, Lukashkina VA, Chen T, Zhou W, Zhu H, Russell IJ, Holt JR, Géléoc GS (2018) Transgenic Tmc2 expression preserves inner ear hair cells and vestibular function in mice lacking Tmc1. Sci Rep 8:12124.

Assad JA, Shepherd GM, Corey DP (1991) Tip-link integrity and mechanical transduction in vertebrate hair cells. Neuron 7:985–994.

Barta CL, Liu H, Chen L, Giffen KP, Li Y, Kramer KL, Beisel KW, He DZ (2018) RNA-seq transcriptomic analysis of adult zebrafish inner ear hair cells. Sci Data 5:180005.

Beck JC, Gilland E, Tank DW, Baker R (2004) Quantifying the ontogeny of optokinetic and vestibuloocular behaviors in zebrafish, medaka, and goldfish. J Neurophysiol 92:3546–3561.

Bedell VM, Ekker SC (2015) Using engineered endonucleases to create knockout and knockin zebrafish models. Methods Mol Biol 1239:291–305.

Bedell VM, Wang Y, Campbell JM, Poshusta TL, Starker CG, Krug RG, Tan W, Penheiter SG, Ma AC, Leung AY, Fahrenkrug SC, Carlson DF, Voytas DF, Clark KJ, Essner JJ, Ekker SC (2012) In vivo genome editing using a high-efficiency TALEN system. Nature 491:114–118.

Beurg M, Fettiplace R, Nam JH, Ricci AJ (2009) Localization of inner hair cell mechanotransducer channels using high-speed calcium imaging. Nat Neurosci 12:553–558.

Beurg M, Kim KX, Fettiplace R (2014) Conductance and block of hair-cell mechanotransducer channels in transmembrane channel-like protein mutants. J Gen Physiol 144:55–69.

Beurg M, Goldring AC, Fettiplace R (2015a) The effects of Tmc1 Beethoven mutation on mechanotransducer channel function in cochlear hair cells. J Gen Physiol 146:233–243.

Beurg M, Xiong W, Zhao B, Müller U, Fettiplace R (2015b) Subunit determination of the conductance of hair-cell mechanotransducer channels. Proc Natl Acad Sci USA 112:1589–1594.

Beurg M, Cui R, Goldring AC, Ebrahim S, Fettiplace R, Kachar B (2018) Variable number of TMC1-dependent mechanotransducer channels underlie tonotopic conductance gradients in the cochlea. Nat Commun 9:2185.

Beurg M, Barlow A, Furness DN, Fettiplace R (2019) A Tmc1 mutation reduces calcium permeability and expression of mechanoelectrical transduction channels in cochlear hair cells. Proc Natl Acad Sci USA 116:20743–20749.

Chen Z, Zhu S, Kindig K, Wang S, Chou SW, Davis RW, Dercoli MR, Weaver H, Stepanyan R, McDermott BM (2020) Tmc proteins are essential for zebrafish hearing where Tmc1 is not obligatory. Hum Mol Genet Advance online publication. Retrieved March 13, 2020. doi: 10.1093/hmg/ddaa045.

Chou SW, Chen Z, Zhu S, Davis RW, Hu J, Liu L, Fernando CA, Kindig K, Brown WC, Stepanyan R, McDermott BM (2017) A molecular basis for water motion detection by the mechanosensory lateral line of zebrafish. Nat Commun 8:2234.

Corey DP, Hudspeth AJ (1979) Ionic basis of the receptor potential in a vertebrate hair cell. Nature 281:675–677.

Corns LF, Johnson SL, Kros CJ, Marcotti W (2016) Tmc1 point mutation affects Ca^{2+} sensitivity and block by dihydrostreptomycin of the mechanoelectrical transducer current of mouse outer hair cells. J Neurosci 36:336–349.

Easter SS, Nicola GN (1997) The development of eye movements in the zebrafish (*Danio rerio*). Dev Psychobiol 31:267–276.

Einhorn Z, Trapani JG, Liu Q, Nicolson T (2012) Rabconnectin3α promotes stable activity of the H^+ pump on synaptic vesicles in hair cells. J Neurosci 32:11144–11156.

Erickson T, Morgan CP, Olt J, Hardy K, Busch-Nentwich E, Maeda R, Clemens R, Krey JF, Nechiporuk A, Barr-Gillespie PG, Marcotti W, Nicolson T (2017) Integration of Tmc1/2 into the mechanotransduction complex in zebrafish hair cells is regulated by transmembrane O-methyltransferase (Tomt). Elife 6:28474.

Faul F, Erdfelder E, Lang AG, Buchner A (2007) G*Power 3: a flexible statistical power analysis program for the social, behavioral, and biomedical sciences. Behav Res Methods 39:175–191.

Fettiplace R, Nam JH (2019) Tonotopy in calcium homeostasis and vulnerability of cochlear hair cells. Hear Res 376:11–21.

Gale JE, Marcotti W, Kennedy HJ, Kros CJ, Richardson GP (2001) FM 1-43 dye behaves as a permeant blocker of the hair-cell mechanotransducer channel. J Neurosci 21:7013–7025.

Gleason MR, Nagiel A, Jamet S, Vologodskaia M, López-Schier H, Hudspeth AJ (2009) The transmembrane inner ear (Tmie) protein is essential for normal hearing and balance in the zebrafish. Proc Natl Acad Sci USA 106:21347–21352.

Goldring AC, Beurg M, Fettiplace R (2019) The contribution of TMC1 to adaptation of mechanoelectrical transduction channels in cochlear outer hair cells. J Physiol 597:5949–5961.

Géléoc GS, Holt JR (2003) Developmental acquisition of sensory transduction in hair cells of the mouse inner ear. Nat Neurosci 6:1019–1020.

Hudspeth AJ (1982) Extracellular current flow and the site of transduction by vertebrate hair cells. J Neurosci 2:1–10.

Hwang WY, Fu Y, Reyon D, Maeder ML, Kaini P, Sander JD, Joung JK, Peterson RT, Yeh JR (2013a) Heritable and precise zebrafish genome editing using a CRISPR-Cas system. PLoS One 8:e68708.

Hwang WY, Fu Y, Reyon D, Maeder ML, Tsai SQ, Sander JD, Peterson RT, Yeh JR, Joung JK (2013b) Efficient genome editing in zebrafish using a CRISPR-Cas system. Nat Biotechnol 31:227–229.

Indzhykulian AA, Stepanyan R, Nelina A, Spinelli KJ, Ahmed ZM, Belyantseva IA, Friedman TB, Barr-Gillespie PG, Frolenkov GI (2013) Molecular remodeling of tip-links underlies mechanosensory regeneration in auditory hair cells. PLoS Biol 11:e1001583.

Jia Y, Zhao Y, Kusakizako T, Wang Y, Pan C, Zhang Y, Nureki O, Hattori M, Yan Z (2020) TMC1 and TMC2 proteins are pore-forming subunits of mechanosensitive ion channels. Neuron 105:310–321.e3.

Kawashima Y, Kurima K, Pan B, Griffith AJ, Holt JR (2015) Transmembrane channel-like (TMC) genes are required for auditory and vestibular mechanosensation. Pflugers Arch 467:85–94.

Kawashima Y, Géléoc GS, Kurima K, Labay V, Lelli A, Asai Y, Makishima T, Wu DK, Della Santina CC, Holt JR, Griffith AJ (2011) Mechanotransduction in mouse inner ear hair cells requires transmembrane channel-like genes. J Clin Invest 121:4796–4809.

Kazmierczak P, Sakaguchi H, Tokita J, Wilson-Kubalek EM, Milligan RA, Müller U, Kachar B (2007) Cadherin 23 and protocadherin 15 interact to form tip-link filaments in sensory hair cells. Nature 449:87–91.

Kettleborough RN, Busch-Nentwich EM, Harvey SA, Dooley CM, de Bruijn E, van Eeden F, Sealy I, White RJ, Herd C, Nijman IJ, Fényes F, Mehroke S, Scahill C, Gibbons R, Wali N, Carruthers S, Hall A, Yen J, Cuppen E, Stemple DL (2013) A systematic genome-wide analysis of zebrafish protein-coding gene function. Nature 496:494–497.

Kindt KS, Finch G, Nicolson T (2012) Kinocilia mediate mechanosensitivity in developing zebrafish hair cells. Dev Cell 23:329–341.

Kurima K, Ebrahim S, Pan B, Sedlacek M, Sengupta P, Millis BA, Cui R, Nakanishi H, Fujikawa T, Kawashima Y, Choi BY, Monahan K, Holt JR, Griffith AJ, Kachar B (2015) TMC1 and TMC2 localize at the site of mechanotransduction in mammalian inner ear hair cell stereocilia. Cell Rep 12:1606–1617.

Kwan KM, Fujimoto E, Grabher C, Mangum BD, Hardy ME, Campbell DS, Parant JM, Yost HJ, Kanki JP, Chien CB (2007) The Tol2kit: a multisite gateway-based construction kit for Tol2 transposon transgenesis constructs. Dev Dyn 236:3088–3099.

Labun K, Montague TG, Gagnon JA, Thyme SB, Valen E (2016) CHOPCHOP v2: a web tool for the next generation of CRISPR genome engineering. Nucleic Acids Res 44:W272–W276.

Labun K, Montague TG, Krause M, Torres Cleuren YN, Tjeldnes H, Valen E (2019) CHOPCHOP v3: expanding the CRISPR web toolbox beyond genome editing. Nucleic Acids Res 47:W171–W174.

Lanford PJ, Popper AN (1996) Novel afferent terminal structure in the crista ampullaris of the goldfish, carassius auratus. J Comp Neurol 366:572–579.

Lu Z, DeSmidt AA (2013) Early development of hearing in zebrafish. J Assoc Res Otolaryngol 14:509–521.

Maeda R, Pacentine IV, Erickson T, Nicolson T (2017) Functional analysis of the transmembrane and cytoplasmic domains of Pcdh15a in zebrafish hair cells. J Neurosci 37:3231–3245.

Maeda R, Kindt KS, Mo W, Morgan CP, Erickson T, Zhao H, Clemens-Grisham R, Barr-Gillespie PG, Nicolson T (2014) Tip-link protein protocadherin 15 interacts with transmembrane channel-like proteins TMC1 and TMC2. Proc Natl Acad Sci USA 111:12907–12912.

Mahendrasingam S, Furness DN (2019) Ultrastructural localization of the likely mechanoelectrical transduction channel protein, transmembrane-

like channel 1 (TMC1) during development of cochlear hair cells. Sci Rep 9:1274.

Mahendrasingam S, Fettiplace R, Alagramam KN, Cross E, Furness DN (2017) Spatiotemporal changes in the distribution of LHFPL5 in mice cochlear hair bundles during development and in the absence of PCDH15. PLoS One 12:e0185285.

Mo W, Chen F, Nechiporuk A, Nicolson T (2010) Quantification of vestibular-induced eye movements in zebrafish larvae. BMC Neurosci 11:110.

Montague TG, Cruz JM, Gagnon JA, Church GM, Valen E (2014) CHOPCHOP: a CRISPR/Cas9 and TALEN web tool for genome editing. Nucleic Acids Res 42:W401–W407.

Nakanishi H, Kurima K, Kawashima Y, Griffith AJ (2014) Mutations of TMC1 cause deafness by disrupting mechanoelectrical transduction. Auris Nasus Larynx 41:399–408.

Nakanishi H, Kurima K, Pan B, Wangemann P, Fitzgerald TS, Géléoc GS, Holt JR, Griffith AJ (2018) Tmc2 expression partially restores auditory function in a mouse model of DFNB7/B11 deafness caused by loss of Tmc1 function. Sci Rep 8:12125.

Ó Maoiléidigh D, Ricci AJ (2019) A bundle of mechanisms: inner-ear hair-cell mechanotransduction. Trends Neurosci 42:221–236.

Pacentine IV, Nicolson T (2019) Subunits of the mechano-electrical transduction channel, Tmc1/2b, require Tmie to localize in zebrafish sensory hair cells. PLoS Genet 15:e1007635.

Pan B, Géléoc GS, Asai Y, Horwitz GC, Kurima K, Ishikawa K, Kawashima Y, Griffith AJ, Holt JR (2013) TMC1 and TMC2 are components of the mechanotransduction channel in hair cells of the mammalian inner ear. Neuron 79:504–515.

Pan B, Akyuz N, Liu XP, Asai Y, Nist-Lund C, Kurima K, Derfler BH, György B, Limapichat W, Walujkar S, Wimalasena LN, Sotomayor M, Corey DP, Holt JR (2018) TMC1 forms the pore of mechanosensory transduction channels in vertebrate inner ear hair cells. Neuron 99:736–753.

Pickles JO, Comis SD, Osborne MP (1984) Cross-links between stereocilia in the guinea pig organ of Corti, and their possible relation to sensory transduction. Hear Res 15:103–112.

Popper A (1977) A scanning electron microscopic study of the sacculus and lagena in the ears of fifteen species of teleost fishes. J Morphol 153:397–417.

Popper AN (2000) Hair cell heterogeneity and ultrasonic hearing: recent advances in understanding fish hearing. Philos Trans R Soc Lond B Biol Sci 355:1277–1280.

Scheffer DI, Shen J, Corey DP, Chen ZY (2015) Gene expression by mouse inner ear hair cells during development. J Neurosci 35:6366–6380.

Seiler C, Nicolson T (1999) Defective calmodulin-dependent rapid apical endocytosis in zebrafish sensory hair cell mutants. J Neurobiol 41:424–434.

Sugihara I, Furukawa T (1989) Morphological and functional aspects of two different types of hair cells in the goldfish sacculus. J Neurophysiol 62:1330–1343.

Westerfield M (2000) The zebrafish book. A guide for the laboratory use of zebrafish (Danio rerio), Ed 4. Eugene, OR: University of Oregon.

Xiong W, Grillet N, Elledge HM, Wagner TF, Zhao B, Johnson KR, Kazmierczak P, Müller U (2012) TMHS is an integral component of the mechanotransduction machinery of cochlear hair cells. Cell 151:1283–1295.

Zhao B, Wu Z, Grillet N, Yan L, Xiong W, Harkins-Perry S, Müller U (2014) TMIE is an essential component of the mechanotransduction machinery of cochlear hair cells. Neuron 84:954–967.